The use of contrast enhancement techniques in X-ray imaging of lithium–ion battery electrodes

Oluwadamilola O. Taiwo [a], Donal P. Finegan [a], Jeff Gelb [b], Christian Holzner [b], Daniel J.L. Brett [a], Paul R. Shearing [a,*]

[a] *The Electrochemical Innovation Lab, Department of Chemical Engineering, University College London, WC1E 7JE, UK*
[b] *Carl Zeiss X-ray Microscopy Inc., Pleasanton, CA 94588, USA*

HIGHLIGHTS

- Micro- and nano-scale XRM were used to characterize a Li-ion graphite electrode.
- Enhanced X-ray image contrast was obtained by signal blending and optimization.
- Imaging resolution requirement varied with the investigated electrode parameter.

ARTICLE INFO

ABSTRACT

Understanding the microstructural morphology of Li–ion battery electrodes is crucial to improving the electrochemical performance of current Li–ion battery systems and in developing next-generation power systems. The use of 3D X-ray imaging techniques, which are continuously evolving, provides a non-invasive platform to study the relationship between electrode microstructure and performance at various time and length scales. In addition to characterizing a weakly (X-ray) absorbing graphite electrode at multiple length scales, we implement an approach for obtaining improved nano-scale image contrast on a laboratory X-ray microscope by combining information obtained from both absorption–contrast and Zernike phase-contrast X-ray images.

1. Introduction

Li-ion batteries have achieved widespread use in a variety of electronic applications, ranging from portable consumer electronic devices to electric vehicles and aircraft to grid storage applications. Electrochemical reactions which take place within Li–ion batteries are supported by porous composite electrodes, which consist mainly of particles of active material mixed with a conductive material and binder. The microstructure of these electrodes is inherently three-dimensional and has a strong influence on battery performance metrics such as durability, capacity retention, cyclability, and safety.

In recent years, the understanding of the microstructure within electrochemical devices has been revolutionized through the use of tomographic imaging techniques, mainly using X-rays (Ebner et al., 2013; Shearing et al., 2010a, 2010b; Yan et al., 2012) and focused-ion beam milling (Ender et al., 2011; Hutzenlaub et al., 2014; Wilson et al., 2011). Although destructive in operation, focused-ion beam tomography techniques provide sufficiently high resolution (typically < 100 nm) and contrast suitable for understanding nano-scale properties within a porous electrode. X-ray computed tomography (CT) is a diagnostic tool that has been used to non-invasively explore a variety of real-life electro-active materials, thus providing unique insight not only into their complex, three-dimensional nature but also on their degradation, aging, and failure upon reaction or during device operation (Finegan et al., 2015a, 2015b; Yufit et al., 2011).

Tomographic imaging has been used to examine battery cathode materials, even at multiple length scales (Shearing et al., 2012); however, for low atomic number (low-Z) anode materials (e.g. graphite), conventional tomographic imaging approaches have some limitations. For instance, the Ga^+ focused-ion beam interacts with graphitic structures, often resulting in highly non-uniform surface milling; moreover, with conventional absorption contrast X-ray imaging, it is difficult to obtain high-contrast images due to the extremely small X-ray absorption coefficients of low-Z materials, especially at the nanometer length scale.

* Corresponding author.
E-mail address: p.shearing@ucl.ac.uk (P.R. Shearing).

The proliferation of phase-contrast X-ray imaging modalities (Davis et al., 1995; Holzner et al., 2010; Irvine et al., 2014; Schmahl et al., 1994; Wilkins et al., 1996) has helped enhance contrast in X-ray images of weakly absorbing materials by utilizing phase shifts across the incident X-ray beam. For nanoscale imaging in particular, Zernike phase contrast X-ray imaging has been used to improve the contrast in CT images of graphite anodes (Eastwood et al., 2014) and of the conductive additive-binder phase in a Li–ion battery cathode (Komini Babu et al., 2015), enhancing the visibility of sub-micron features of interest within the electrode materials. Unfortunately, Zernike phase-contrast tomography on low-Z materials produces undesired artifacts, such as "halos" and "shade-off" (Otaki, 2000), which preclude the use of traditional image segmentation techniques that employ a single value threshold; however, images laden with such artifacts may be restored with use of algorithms which model the phase contrast optics (Kumar et al., 2015).

To address this problem, we develop and apply a combined contrast approach to characterize the three-dimensional (3D) microstructure in a graphite-based electrode material using image information obtained subsequently from both absorption–contrast and phase-contrast X-ray CT imaging. Previously, Komini Babu and co-workers (Komini Babu et al., 2015) successfully used Zernike phase-contrast and absorption–contrast X-ray CT imaging to separately resolve the active material and carbon-binder phases in a LiCoO$_2$ cathode material by merging the resulting segmented image data from both X-ray CT images with mathematical image operations. However, we have demonstrated the combination of absorption and phase contrast information from sequential X-ray imaging in a laboratory X-ray microscope without prior image segmentation by blending and optimizing the weighting of the signal from both X-ray images in order to create a final enhanced image with improved contrast. This technique leverages the benefits of both phase and absorption imaging: maintaining the fine detail of electrode cracks characteristic of phase images with the ease of image analysis of absorption imaging, which enables the use of single-threshold image segmentation and minimal post-processing of image reconstructions.

Here, we also present microstructural investigations at two length scales, using laboratory X-ray Microscopy (XRM) to image the bulk electrode and to identify a region of interest for subsequent investigation using nano-scale XRM. For the first time, we present the results of high-resolution studies on a graphite anode material using our unique combined phase/absorption approach.

2. Materials and methods

Graphite electrodes were prepared by mixing graphite powder (TIMREX® SLP30, TIMCAL, Switzerland), carbon black (Super P, Sigma Aldrich, UK), and PVDF binder (Pi-KEM, UK) in the respective percentage weight ratios 87:3:10 with n-methyl-pyrrolidone (Pi-KEM, UK) in a mixer (ULTRA-TURRAX, IKA-Werke GmbH, Germany). The resulting slurry was dried at 80 °C under vacuum for 24 h. The surface morphology of the prepared electrode was captured using scanning electron microscopy (ZEISS EVO MA 10, ZEISS, USA).

X-ray microscopy, or XRM, is an imaging technique that employs digital geometry processing to reconstruct a 3D image of the internal structure of an object from a series of two-dimensional (2D) X-ray projection images, which are recorded as the object is rotated about a single axis. When X-rays are incident upon an object, they are absorbed, transmitted, and/or scattered. In standard X-ray computed tomography (X-ray CT), the 2-D projection images are progressively obtained by passing a beam of X-rays from an X-ray source through the sample object as it is rotated at certain angular increments. The transmitted X-rays are then recorded by an X-ray detection system, in which the beam of high-energy photons is converted to visible light by a scintillator, imaged through an objective lens onto a CCD detector and read out into a computer for further processing. A 3D digital image of the object is then created by mathematically reconstructing the acquired series of 2D projection images where each voxel (volume element or 3D pixel) represents the X-ray absorption at that point.

Following electrode preparation, the three-dimensional microstructure of an electrode sample was examined using two X-ray tomography platforms: laboratory-based micron-scale XRM (ZEISS Xradia Versa 520, Carl Zeiss X-ray Microscopy Inc., Pleasanton, CA) and nano-scale XRM (ZEISS Xradia 810 Ultra, Carl Zeiss X-ray Microscopy Inc., Pleasanton, CA). Schematic representations of the micro-XRM and nano-XRM imaging setups are presented in Fig. 1a and b respectively. The micro-XRM system can perform non-destructive 3D X-ray imaging achieving true spatial resolution to
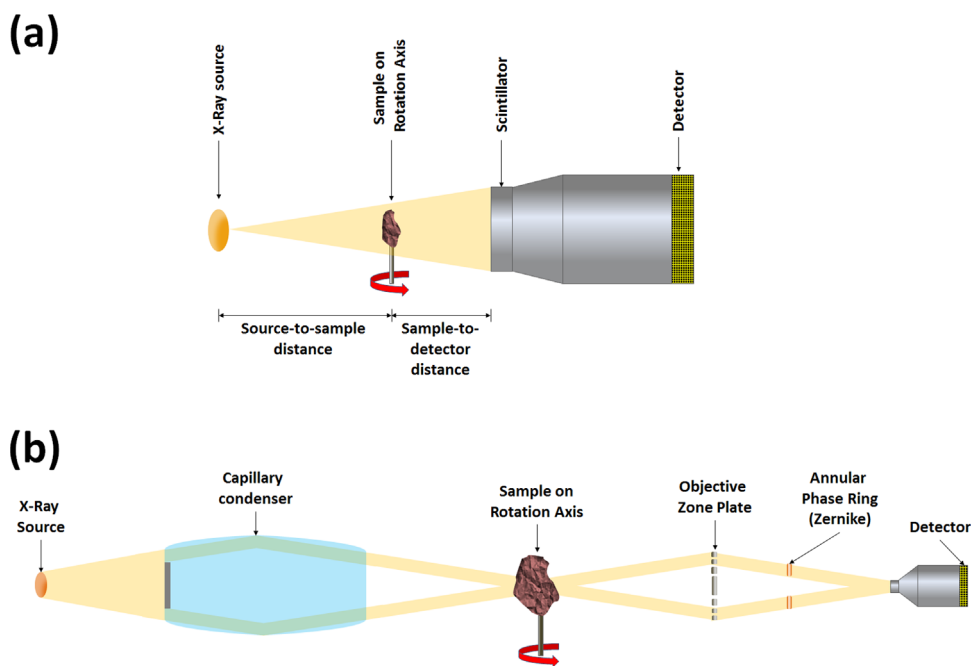

Fig. 1. Schematic of (a) a typical micro-scale laboratory XRM setup and (b) a nano-scale laboratory XRM setup operating in Zernike phase contrast mode.

around 700 nm. The instrument is equipped with a micrometer spot size laboratory X-ray source with cone beam geometry, and a high-resolution optically-coupled detector which can detect the X-rays transmitted through the investigated sample. The nano-XRM system has a much higher resolution, achieving resolutions as fine as 50 nm; the system also possesses both absorption and Zernike phase contrast capabilities to enable non-invasive imaging of a variety of materials at the nanometer scale. The coupling of these systems enables multi-scale insight into the microstructure of battery electrodes, which can be used to optimize materials design and manufacturing for high performance cells.

3D datasets were collected at 20X optical magnification in absorption–contrast mode using the micron-scale XRM instrument. To obtain a good signal-to-noise ratio, a total of 3201 radiographs were acquired over a 360° sample rotation range with an exposure time of 40 s per radiograph. The electrode sample was placed between the X-ray source and a $2k \times 2k$ detector with a source–detector distance of 23.6 mm providing a voxel resolution of $\sim$670 nm with the detector set to 2×2 pixel binning.

After the micron-scale analysis, the graphite electrode sample was then carefully dissected with a scalpel into smaller samples sizes for nano-CT studies (Shearing et al., 2010a). For the nano-scale XRM experiments, both absorption–contrast and phase-contrast images of the graphite electrode were acquired in the "large field-of-view" mode (with a field–of–view of 65 µm × 65 µm in dimension). A total of 1601 projections were collected per 180° sample rotation with an exposure time of 3 s for the absorption–contrast imaging and 8 s for the phase-contrast imaging. This yielded two sets of raw image data, both with an isotropic voxel resolution of $\sim$130 nm using a detector pixel binning of 2.

In order to generate a nano-scale data set of the graphite electrode sufficient enough for some microstructural quantification, 'mosaic imaging' was carried out whereby separate XRM images of adjacent field of views were successively acquired and then stitched together to form taller single tomographic image using a commercial tomographic image stitching algorithm (Vertical Stitching plugin, Carl Zeiss X-ray Microscopy Inc., USA); this enabled imaging of samples which are taller or wider than the X-ray instrument's standard field of view. Phase-contrast and absorption–contrast images were collected for each region of interest to achieve contrast-enhanced reconstructions. In order to enable adequate execution of the image stitching procedure, a vertical overlap of 15% between the field of view of both image scans was applied.

The raw transmission images from both micro- and nano-scale XRM imaging experiments were reconstructed using a commercial image reconstruction software package (ZEISS XMReconstructor, Carl Zeiss X-ray Microscopy Inc., Pleasanton, CA) which employs a filtered back-projection algorithm. Tomographic scan details are shown in Table 1.

Table 1
Tomography acquisition details.

| Scan parameter	Micro-XRM	Nano-XRM	
Contrast mode	Absorption	Phase	Absorption
Source voltage (kV) or Photon energy (keV)	30 kV	5.4 keV	5.4 keV
Camera binning	2	2	2
Number of projections	3201	1601	1601
Radiograph exposure time (s)	40	8	3
Voxel size (nm)	670	130	130
Magnification/Field-of-view (FOV)	20X	Large FOV	Large FOV

3. Results and discussion

Scanning electron micrographs of the prepared electrode (Fig. 2) revealed a platelet–like shape of the graphite particles, defects on particle surfaces, particle arrangement mostly along the graphite particle basal plane, and a nearly uniform particle size distribution. Whilst the micrographs show a wealth of qualitative structural information, SEM imaging is limited in its ability to provide accurate quantitative information on inherently three-dimensional structural parameters, such as tortuosity and pore-phase connectivity. These parameters directly influence the performance of the electrode in the cell, thus motivating material microstructural studies in three dimensions (Kehrwald et al., 2011).

The reconstructed 3D image volume from the micron-scale XRM imaging was segmented using the Avizo software package (Avizo 9.0, FEI Visualization Sciences Group, Mérignac Cedex, France). The reconstructed volume showed a high signal-to-noise ratio due to the large number of projection images (Fig. 3a) collected during the CT scan, thus making image segmentation straightforward. Fig. 3b and c show a single reconstructed grey-scale 2D slice of graphite electrode and the resulting binary image from segmenting the solid electrode and pore phases. A representative region of interest (ROI) was then extracted from the full micro-XRM 3D data-set by cropping a volume of interest (ca. 447 µm × 402 µm × 65 µm) which fulfilled representative volume element conditions (Taiwo et al., 2016) for subsequent analysis. From the nano-XRM mosaic imaging, a reconstructed volume of ca. 43 µm × 98 µm × 41 µm was extracted for further analysis.

X-ray radiographs from nano-scale XRM imaging in absorption and Zernike phase-contrast imaging modes are presented in Fig. 5a and b respectively, and resulting reconstructed slices in Fig. 5c and d. From the radiographs, it can clearly be seen that the Zernike phase contrast imaging enhances features and edges of the graphite electrode particles compared to the absorption–contrast imaging; this is also observed in the reconstructed images. Each image has its merits: the phase-contrast image provides more boundary edge contrast information, revealing the internal inclusions and cracks in the graphite microstructure, while the absorption–contrast image represents density information, which is particularly important for reliable, automated image segmentation. In order to take advantage of the merits of both imaging techniques, the contrast information from both absorption–contrast and phase-contrast images was merged to yield a "combined contrast" image (Fig. 5e); this was performed using image
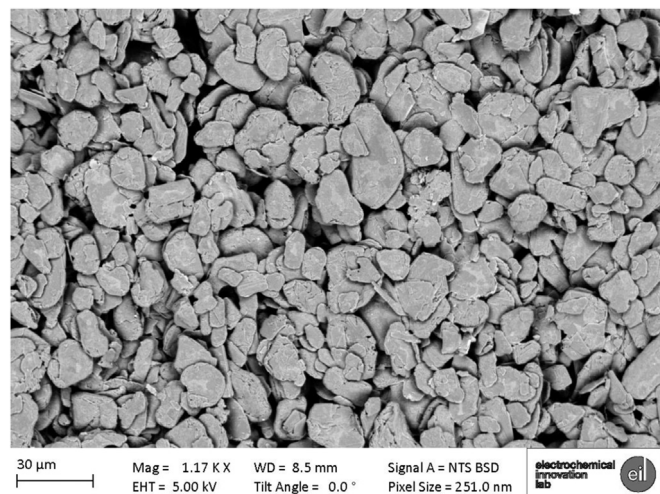
Fig. 2. Scanning electron micrograph of the prepared graphite electrode.
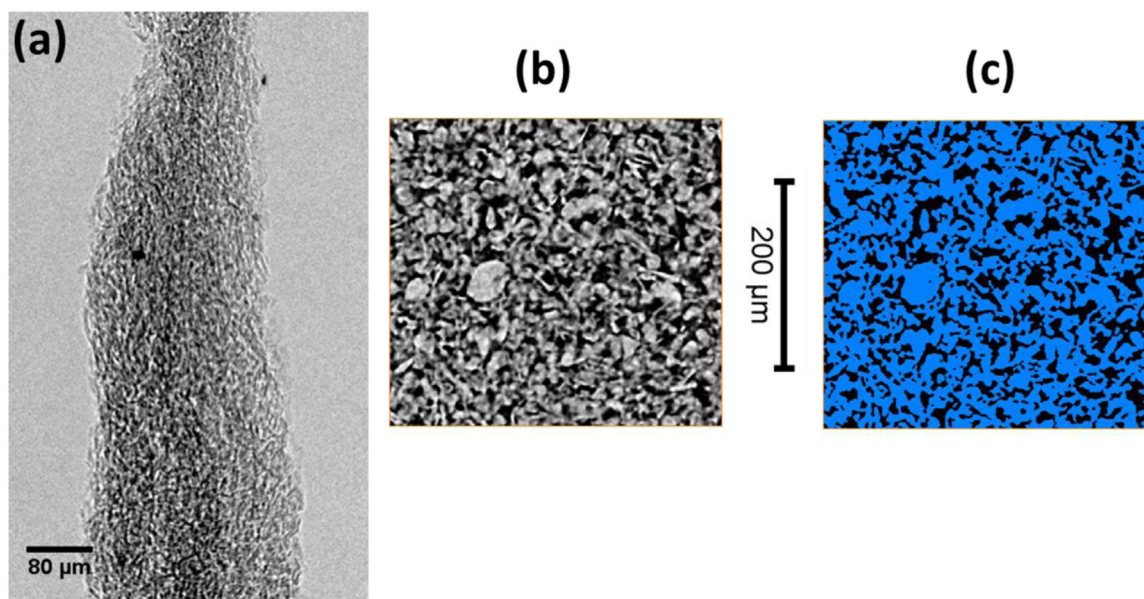
Fig. 3. (a) A single X-ray projection image of the graphite electrode material acquired from absorption–contrast micron-scale XRM. (b) A single 2D reconstructed slice of a cropped region of interest from the micro-XCT graphite 3D greyscale data set and (c) the resulting binarized image.

registration and dual–scan analysis with the aid of a commercial software package for signal blending and contrast optimization of XRM images (Carl Zeiss X-ray Microscopy, 2014; Case et al., 2015).
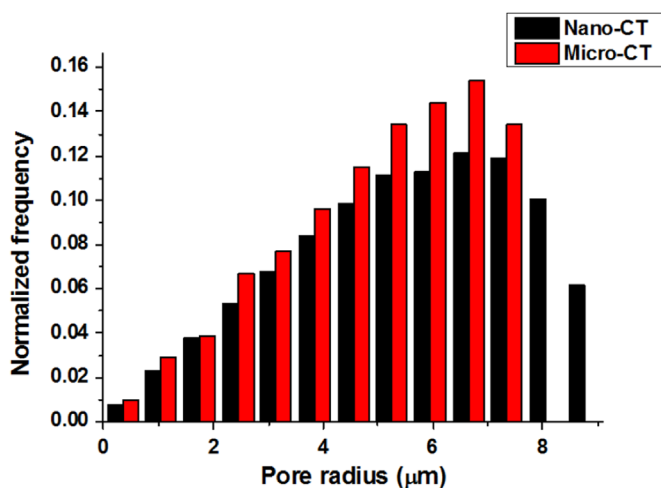
Most commonly used in dual-energy imaging [see e.g. (Zhu et al., 2015)], the dual-scan analysis software enables blending of the absorption and phase contrast images by aid of a two-dimensional intensity histogram, with the goal to preserve the favorable contrast behavior of the two imaging modes; edge

Fig. 4. Pore size distribution extracted from the nano-XRM and micro-XRM image datasets.

enhancement from phase contrast and density information from absorption.

The variations of greyscale intensity across the graphite particles can significantly determine threshold segmentation accuracy. The 2D histogram of a line profile across a graphite particle in the reconstructed image (Fig. 6) was plotted for all three acquired images. With the phase-contrast image, the histogram clearly shows that the graphite particle boundary edges can be clearly mapped by the presence of distinct intensity fringes (unlike in the absorption-contrast image); however, a complete and accurate

threshold-based segmentation of the graphite particle based solely on the phase information will prove troublesome due to the presence of shade-off (i.e. due to the similarities in the greyscale intensity within the graphite particle interior and exterior).

The absorption–contrast image, however, shows a substantial attenuation contrast distribution between background and the graphite particle, but not as much detail on particle defects and boundary edges as the phase-contrast image. As highlighted in Fig. 6, sub-particle defects, visible in phase contrast, are difficult to detect from the absorption contrast data set alone. Combining boundary edge and attenuation information from both phase-contrast and absorption-contrast images provides a sufficient distribution of greyscale intensity to ease automated threshold-based segmentation whilst maintaining the unique benefits of phase contrast imaging to describe physical edges and cracks in the electrode. Image segmentation of the combined nano-scale XRM dataset was also performed in Avizo software and volume renderings resulting from the enhanced contrast image are shown in Fig. 5f and g.

Quantitative analysis was performed on the micron- and enhanced nano-scale XRM data sets to extract microstructural parameters: namely, porosity, volume-specific surface area, pore-phase tortuosity, and mean pore size (see Table 2). Porosity and volume-specific surface area were calculated in Avizo; specific surface area calculations were based on a marching cubes algorithm (Lorensen and Cline, 1987) with surface mesh smoothing and refinement. Mean pore size was calculated in ImageJ (http://rsbweb.nih.gov/ij/) using a continuous pore size distribution method (Münch and Holzer, 2008), which geometrically calculated the pore size distribution of the 3D porous microstructure by mimicking mercury intrusion porosimetry (MIP). Tortuosity was calculated geometrically with the aid of a fast marching algorithm (Hassouna and Farag, 2007; Jørgensen et al., 2011) implemented in Matlab.
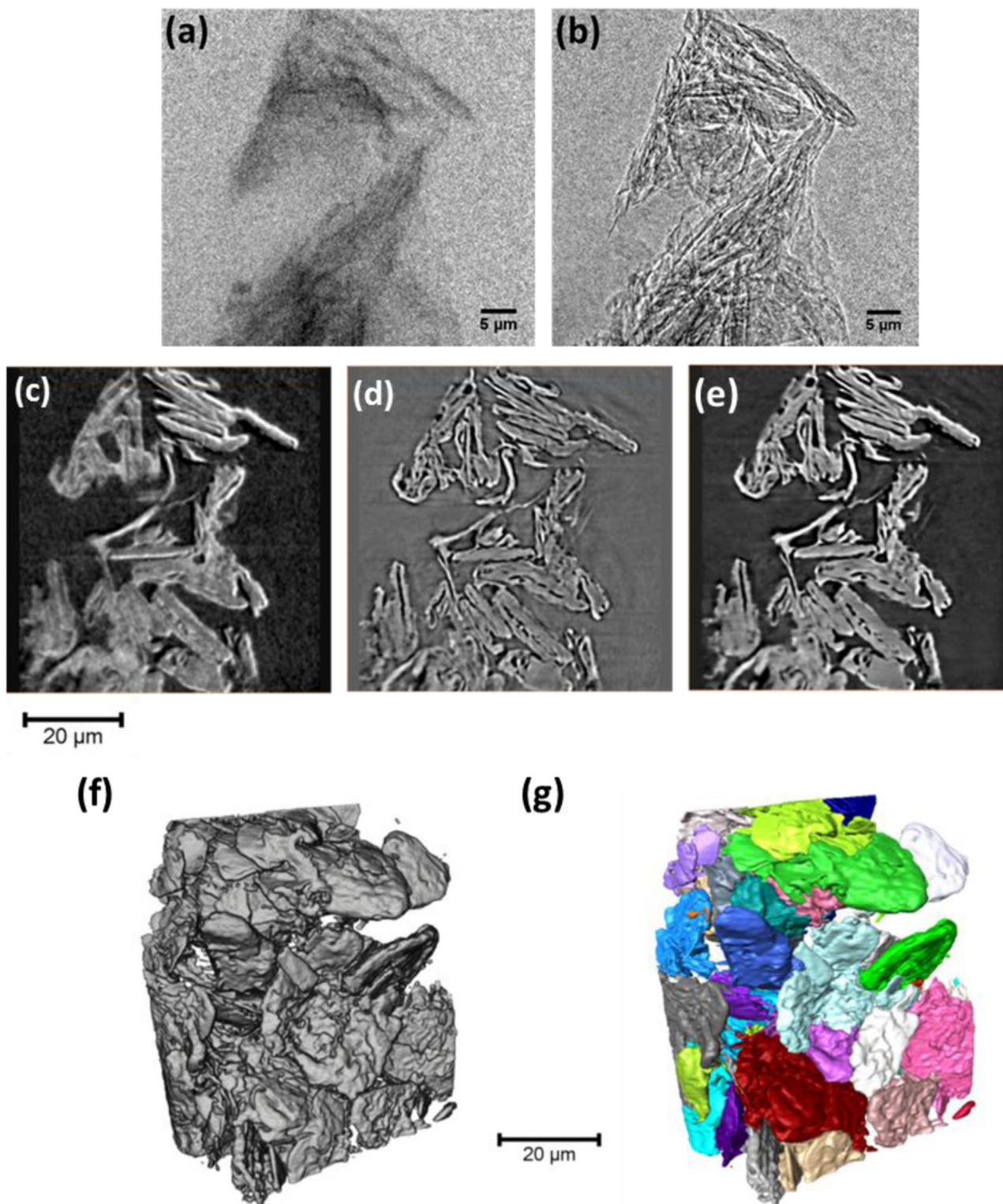
The results, however, show similar porosity, directional pore-phase tortuosity, and mean pore size values between the micron- and nano-scale data sets; the pore size distributions extracted from the nano-CT and micro-CT datasets (Fig. 4) are in good agreement, which is a good validation of the similar porosity values obtained for both datasets. However, volume-specific surface area from the nano-scale scan was more than double that obtained

Fig. 5. A single X-ray projection image of a small region of interest within the graphite electrode acquired using (a) absorption–contrast nano-scale XRM, (b) Zernike phase-contrast nano-scale XRM. Single reconstructed slices from nano-scale XRM (c) in absorption–contrast mode (d) in phase-contrast mode, and (e) after combined-contrast enhancement. (f) Resulting volume rendering of the graphite region of interest, and (g) after algorithmic particle separation and identification.
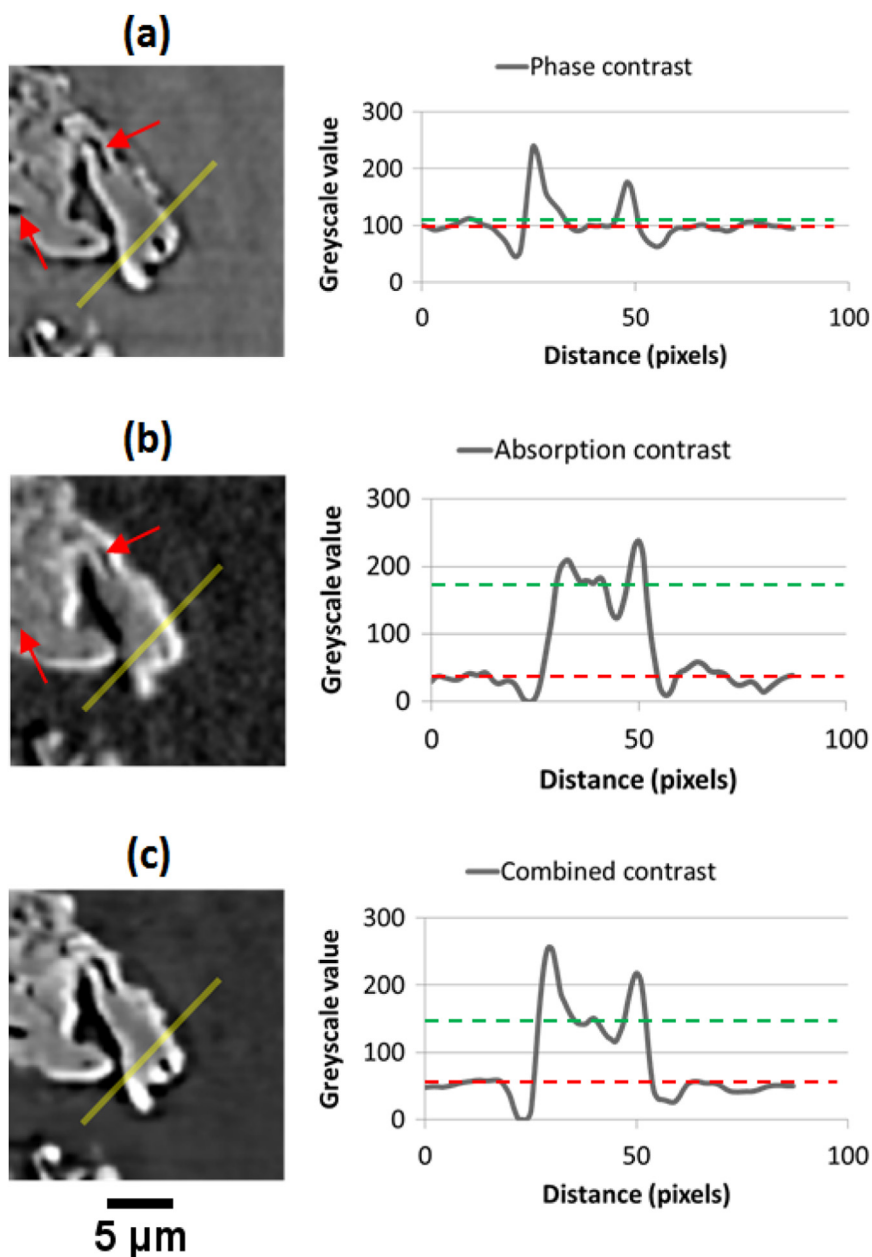
from the micron-scale measurements. This is similar to observations made by the authors in a multi-length scale study of a lithium-manganese-oxide battery cathode material (Shearing et al., 2012), thus reiterating the need for more stringent imaging resolution requirements for surface area measurement studies, which are sensitive to microscopic variations in surface roughness and cracks (Fig. 6).

4. Conclusion

X-ray tomographic imaging enables non-invasive characterization of the complex microstructures within lithium-ion battery electrodes. For low atomic number electrode materials, image segmentation of phase-contrast X-ray images may prove difficult due to insufficient attenuation contrast, which is usually present in

Table 2
Electrode microstructural parameters extracted from tomography data.

Imaging platform	Pixel size (μm)	Porosity (%)	Geometric Tortuosity			Specific surface area (μm^{-1})	Average pore size (μm)
Micro–XRM	0.670	42.52	x	y	z	0.411	2.71
			1.09	1.05	1.26		
Nano–XRM	0.130	42.95	x	y	z	0.861	2.01
			1.14	1.17	1.32		

Fig. 6. Variation in greyscale intensity across a graphite particle in reconstructed images generated from (a) phase contrast imaging, (b) absorption contrast imaging and (c) combined contrast enhancement. Improved attenuation information and boundary edge detection is achieved with the combined contrast image, easing image segmentation. Red arrows highlight particle inclusions and cracks which are visible in Zernike phase-contrast image but not as clear in absorption–contrast image. In each graph, the green and red dashed-lines mark the average greyscale within the graphite particle and background respectively. (For interpretation of the references to color in this figure legend, the reader is referred to the web version of this article.)

absorption–contrast images. Here, for the first time, we combine nano-scale X-ray absorption contrast and phase-contrast X-ray image data of a graphite electrode material for lithium-ion batteries, allowing detailed complementary image information to be gathered which enabled straightforward image analysis that so far was extremely difficult to do. The approach uses an image signal

blending and contrast optimization software to solve a fundamental imaging challenge of X-ray image contrast quality. Using contrast enhancement and vertical tomography stitching algorithms, we were able to generate 3D nano-scale reconstructions of the electrode that give an enhanced image with improved contrast and boundary edge information. We also performed multi-scale

investigations of the electrode material using laboratory micro- and nano-scale XRM, and results from subsequent quantitative analysis showed that, depending on the electrode microstructural parameter under investigation, there is a variation in the imaging resolution and representative volume element requirements.

This technique will significantly improve our understanding of the nano-scale structure of graphite electrodes for Li-ion batteries, and we predict it will find widespread application in a diverse range of low-atomic number materials, which are characteristically challenging to image by absorption contrast alone.

Acknowledgments

References

Carl Zeiss X-ray Microscopy, 2014. Dual Scan Contrast Visualizer (DSCoVer), version 10.7.3245. URL: ⟨http://www.zeiss.com/microscopy/en_de/products/x-ray-microscopy/zeiss-xradia-520-versa.html#highlights⟩ (accessed 27.12.15).

Case, T.A., Candell, S., Seshadri, S., McGuinness, P., 2015. Multi energy X-ray microscope data acquisition and image reconstruction system and method. Patent US13768689.

Davis, T.J., Gao, D., Gureyev, T.E., Stevenson, A.W., Wilkins, S.W., 1995. Phase-contrast imaging of weakly absorbing materials using hard X-rays. Nature 373, 595–598. http://dx.doi.org/10.1038/373595a0.

Eastwood, D.S., Bradley, R.S., Tariq, F., Cooper, S.J., Taiwo, O.O., Gelb, J., Merkle, A., Brett, D.J.L., Brandon, N.P., Withers, P.J., Lee, P.D., Shearing, P.R., 2014. The application of phase contrast X-ray techniques for imaging Li-ion battery electrodes. Nucl. Instrum. Methods Phys. Res. Sect. B Beam Interact. Mater. Atoms 324, 118–123. http://dx.doi.org/10.1016/j.nimb.2013.08.066.

Ebner, M., Marone, F., Stampanoni, M., Wood, V., 2013. Visualization and quantification of electrochemical and mechanical degradation in Li Ion batteries. Science . http://dx.doi.org/10.1126/science.1241882.

Ender, M., Joos, J., Carraro, T., Ivers-Tiffée, E., 2011. Three-dimensional reconstruction of a composite cathode for lithium–ion cells. Electrochem. commun. 13, 166–168.

Finegan, D.P., Scheel, M., Robinson, J.B., Tjaden, B., Hunt, I., Mason, T.J., Millichamp, J., Di Michiel, M., Offer, G.J., Hinds, G., Brett, D.J.L., Shearing, P.R., 2015a. In-operando high-speed tomography of lithium–ion batteries during thermal runaway. Nat. Commun. 6, 6924. http://dx.doi.org/10.1038/ncomms7924.

Finegan, D.P., Tudisco, E., Scheel, M., Robinson, J.B., Taiwo, O.O., Eastwood, D.S., Lee, P.D., Di Michiel, M., Bay, B., Hall, S.A., Hinds, G., Brett, D.J.L., Shearing, P.R., 2015b. Quantifying bulk electrode strain and material displacement within lithium batteries via high-speed operando tomography and digital volume correlation. Adv. Sci., 3. http://dx.doi.org/10.1002/advs.201500332.

Hassouna, M.S., Farag, A.A., 2007. Multi-stencils fast marching methods: a highly accurate solution to the eikonal equation on cartesian domains. IEEE Trans. Pattern Anal. Mach. Intell. 29, 1563–1574. http://dx.doi.org/10.1109/TPAMI.2007.1154.

Holzner, C., Feser, M., Vogt, S., Hornberger, B., Baines, S.B., Jacobsen, C., 2010. Zernike phase contrast in scanning microscopy with X-rays. Nat. Phys. 6, 883–887. http://dx.doi.org/10.1038/nphys1765.

Hutzenlaub, T., Thiele, S., Paust, N., Spotnitz, R., Zengerle, R., Walchshofer, C., 2014. Three-dimensional electrochemical Li–ion battery modelling featuring a focused ion-beam/scanning electron microscopy based three-phase reconstruction of a $LiCoO_2$ cathode. Electrochim. Acta 115, 131–139. http://dx.doi.org/10.1016/j.electacta.2013.10.103.

Irvine, S., Mokso, R., Modregger, P., Wang, Z., Marone, F., Stampanoni, M., 2014. Simple merging technique for improving resolution in qualitative single image phase contrast tomography. Opt. Express 22, 27257–27269. http://dx.doi.org/10.1364/OE.22.027257.

Jørgensen, P.S., Hansen, K.V., Larsen, R., Bowen, J.R., 2011. Geometrical characterization of interconnected phase networks in three dimensions. J. Microsc. 244, 45–58. http://dx.doi.org/10.1111/j.1365-2818.2011.03504.x.

Kehrwald, D., Shearing, P.R., Brandon, N.P., Sinha, P.K., Harris, S.J., 2011. Local tortuosity inhomogeneities in a lithium battery composite electrode. J. Electrochem. Soc. 158, A1393. http://dx.doi.org/10.1149/2.079112jes.

Komini Babu, S., Mohamed, A.I., Whitacre, J.F., Litster, S., 2015. Multiple imaging mode X-ray computed tomography for distinguishing active and inactive phases in lithium-ion battery cathodes. J. Power Sources 283, 314–319. http://dx.doi.org/10.1016/j.jpowsour.2015.02.086.

Kumar, A.S., Mandal, P., Zhang, Y., Litster, S., 2015. Image segmentation of nanoscale Zernike phase contrast X-ray computed tomography images. J. Appl. Phys. 117, 183102. http://dx.doi.org/10.1063/1.4919835.

Lorensen, W.E., Cline, H.E., 1987. Marching cubes: a high resolution 3d surface construction algorithm. SIGGRAPH. Comput. Graph. 21, 163–169. http://dx.doi.org/10.1145/37402.37422.

Münch, B., Holzer, L., 2008. Contradicting geometrical concepts in pore size analysis attained with electron microscopy and mercury intrusion. J. Am. Ceram. Soc. 91, 4059–4067. http://dx.doi.org/10.1111/j.1551-2916.2008.02736.x.

Otaki, T., 2000. Artifact halo reduction in phase contrast microscopy using apodization. Opt. Rev. 7, 119–122. http://dx.doi.org/10.1007/s10043-000-0119-5.

Schmahl, G., Rudolph, D., Schneider, G., Guttmann, P., Niemann, B., 1994. Phase-contrast X-ray Microscopy Studies. Optik (Stuttg) 97, 181–182.

Shearing, P.R., Brandon, N.P., Gelb, J., Bradley, R., Withers, P.J., Marquis, A.J., Cooper, S., Harris, S.J., 2012. Multi length scale microstructural investigations of a commercially available Li-Ion battery electrode. J. Electrochem. Soc. 159, A1023–A1027. http://dx.doi.org/10.1149/2.053207jes.

Shearing, P.R., Gelb, J., Brandon, N.P., 2010a. X-ray nano computerised tomography of SOFC electrodes using a focused ion beam sample-preparation technique. J. Eur. Ceram. Soc. 30, 1809–1814. http://dx.doi.org/10.1016/j.jeurceramsoc.2010.02.004.

Shearing, P.R., Howard, L.E., Jørgensen, P.S., Brandon, N.P., Harris, S.J., 2010b. Characterization of the 3-dimensional microstructure of a graphite negative electrode from a Li–ion battery. Electrochem. Commun. 12, 374–377.

Taiwo, O.O., Finegan, D.P., Eastwood, D.S., Fife, J.L., Brown, L.D., Darr, J.A., Lee, P.D., Brett, D.J.L., Shearing, P.R., 2016. Comparison of three-dimensional analysis and stereological techniques for quantifying lithium-ion battery electrode microstructures. J. Microsc. 21, 1–13. http://dx.doi.org/10.1111/jmi.12389.

Wilkins, S.W., Gureyev, T.E., Gao, D., Pogany, A., Stevenson, A.W., 1996. Phase-contrast imaging using polychromatic hard X-rays. Nature 384, 335–338. http://dx.doi.org/10.1038/384335a0.

Wilson, J.R., Cronin, J.S., Barnett, S.A., Harris, S.J., 2011. Measurement of three-dimensional microstructure in a $LiCoO_2$ positive electrode. J. Power Sources.

Yan, B., Lim, C., Yin, L., Zhu, L., 2012. Three dimensional simulation of galvanostatic discharge of $LiCoO_2$ cathode based on X-ray nano-CT images. J. Electrochem. Soc. 159, A1604–A1614. http://dx.doi.org/10.1149/2.024210jes.

Yufit, V., Shearing, P., Hamilton, R.W., Lee, P.D., Wu, M., Brandon, N.P., 2011. Investigation of lithium–ion polymer battery cell failure using X-ray computed tomography. Electrochem. Commun. 13, 608–610.

Zhu, Y., Manske, S.L., Boyd, S.K., 2015. Cartilage imaging of a rabbit knee using dual-energy X-ray microscopy and 1.0 T and 9.4 T magnetic resonance imaging. J. Orthop. Transl. 3, 212–218. http://dx.doi.org/10.1016/j.jot.2015.07.003.